ARTICLE

Amylase-Functionalized Mesoporous Silica Thin Films as Robust Biocatalyst Platforms

Martín G. Bellino,*,† Alberto E. Regazzoni,†,‡ and Galo J. A. A. Soler-Illia†

Gerencia Química, Comisión Nacional de Energía Atómica, Centro Atómico Constituyentes, Avenida General Paz 1499, B1650KNA-San Martín, Argentina, and Instituto Jorge A. Sabato, Universidad Nacional de San Martín, Avenida General Paz 1499, B1650KNA-San Martín, Argentina

ABSTRACT A robust biocatalyst was produced by immobilization of α-amylase into mesoporous silica thin films with local order pore structure and 11 nm pore diameter, supported on glass stripes. The activity of this novel catalyst was evaluated for direct starch degradation. The catalyst films show excellent activity, and enhanced stability with respect to free enzyme at extreme conditions of pH and temperature. In addition, they can be easily separated from the reaction media and reused several times.

KEYWORDS: mesoporous thin films • immobilized enzymes • catalysis • α-amylase • nanoporous

INTRODUCTION

Production of enzymatic catalysts is perhaps the best and oldest example of biomimetism. Enzymes have been used extensively in industry, medicine, waste treatment, etc. Yet, enzymatic catalysis is currently an active area of research being pursued for new and improved performances (1). Immobilization of enzymes in solid matrices is one of the current trends to optimize biocatalytic processes. A large number of anchoring techniques and solid supports are now available for enzyme immobilization (2). Among the various supports, sol−gel-derived matrices seem promising (3). However, because of their small pores, nonuniform pore size distributions, and limited pore connectivity, the resulting biocatalysts show poor reproducibility and performance. In this sense, ordered mesoporous supports, which have well-defined pore structures with narrow pore size distributions and present interconnected pores and large surface areas (4), appear as attractive host matrices for entrapping enzymes (5). To date, most biofunctionalized mesoporous materials are, however, particulate, which renders their application somewhat complex.

Processing of mesoporous materials as thin films opened a wealth of opportunities for supported devices with properties derived from pore size and surface functionalization with organic or biological groups (6). For example, the possibility of supporting enzymes in mesoporous thin films would represent an evolution regarding mesoporous powders, allowing us to leave behind problems related to reagent and product diffusion. In addition, separation of the supported catalyst from the reaction media becomes trivial. Indeed, thin films supported on suitably designed substrates can be kept inside the reaction mixture and easily separated after the completion of the reaction. The advantages would be to reduce production costs by efficient recycling and improved control of the overall process. Nowadays, only a few mesoporous oxide films have been biofunctionalized with enzymes. Mesoporous thin films loaded by enzymes were exploited as electrochemical biosensing devices (7). Just very recently, mesoporous coatings have been used as lipase hosts for catalysis in continuous flow systems (8). Surprisingly, to date, there are no reports about immobilized enzymes in mesoporous thin films for producing biocatalytic strips that can work as portable catalytic stations. In addition, no enzyme-containing thin films capable of efficiently processing a biopolymer have been reported.

In this work, we report the use of mesoporous thin films supported on glass slides as an efficient host matrix for active enzymes. In particular, α-amylase was encapsulated in mesoporous silica thin films and used in the catalytic experiments. Starch degradation was used to determine the activity of the biofunctionalized films. We show here that these biocatalyst strips are facile to prepare, very easy to separate from the reaction mixture, and reusable several times without any significant degradation of the catalytic efficiency. α-Amylase, a well-known enzyme, was selected because it has a wide range of applications, including textile and food industries, effluent treatment, and biochemical diagnostics (9).

EXPERIMENTAL SECTION

Film Synthesis. All reagents were used as received, without further purification. Mesoporous thin films were produced by evaporation-induced self-assembly (10). For this purpose, glass substrates were dip-coated at 40−50% relative humidity (RH) and 1 and 2 mm s^{-1} withdrawal rates. $Si(OEt)_4$ (TEOS) was used as the inorganic precursor, and Pluronics F127 $((EO)_{106}(PO)_{70}(EO)_{106}$, where EO and PO represent ethylene oxide and propylene oxide blocks, respectively, was selected as the polymeric template. TEOS was prehydrolyzed by refluxing for 1 h in a water/ethanol solution; $[H_2O]/[Si] = 1$; $[EtOH]/[TEOS] = 5$. To this prehydrolyzed solution was added surfactant, alcohol, and acidic water in order to prepare the precursor

* Corresponding author. E-mail: mbellino@cnea.gov.ar.
Received for review June 9, 2009 and accepted December 22, 2009
† Centro Atómico Constituyentes.
‡ Universidad Nacional de San Martín.
DOI: 10.1021/am900645b

Published on Web 01/12/2010

solutions, with final composition TEOS:EtOH:H_2O (0.1 M HCl): F127 equal to 1:40:5:0.0075 mol ratios. The relatively large [F127]/[Si] ratio ensures a high accessible porosity.

After deposition by dip-coating, as-prepared films were placed in a 50% RH chamber for 24 h. The films were then subjected to a consolidation thermal treatment, which consisted of heating at 60 °C for 24 h and at 130 °C for another 24 h. Finally, the films were calcined at 350 °C for 2 h in order to remove the template.

For comparison, nonporous films were made as described, but in the absence of the polymeric template.

Film Characterization. Film mesostructure was analyzed by small-angle X-ray scattering (SAXS) at the D02A-SAXS2 line of LNLS, Campinas, SP, Brazil ($\lambda = 1.608$ Å) at normal (90°) and glancing (3°) incidence.

Field emission-scanning electron microscopy (FE-SEM) images were taken with a Zeiss Leo 982 Gemini electron microscope using the secondary-electron mode and an in-lens detector to improve resolution. Transmission electron microscopy (TEM) images were obtained using a Phillips CM 200 electron microscope at an acceleration voltage of 200 kV.

Film electronic density and thickness were determined from the analysis of critical angle and Kiessig fringes by X-ray reflectometry (XRR) measurements (11), performed at the D10A-XRD2 line of Laboratório Nacional de Luz Síncrotron, Campinas, SP, Brazil ($\lambda = 1.5498$ Å). Measurements were carried out at 0% RH to avoid the condensation of water that might bias the density assessment. A SOPRA GES5A apparatus equipped with microsopts was used for optical measurements; film thickness and refractive index were obtained by fitting the measured ellipsometric parameters $\Psi(\lambda)$ and $\Delta(\lambda)$ in the 400−800 nm spectral range for both the supported films and the bare substrate (12). In this range, no light absorption is observed, therefore only the real part of the refractive index (n) is obtained. The model used for fitting consistsed of a thin oxide film supported on glass. The glass and film refractive index were described according to a modified Cauchy equation (i.e., $n(\lambda) = A + (B)/(\lambda^2)$); A and B parameters were extracted from the best fit of $\Psi(\lambda)$ and $\Delta(\lambda)$. Water adsorption isotherms at 298 K were measured by environmental ellipsometric porosimetry (EEP) according to the protocols developed in ref (13). In this technique, a continuous flux of air containing a fixed partial water pressure was put in contact with the mesoporous film to be analyzed. Film thickness and refractive index values were obtained at each relative pressure value, P/P_s, where P is the actual vapor pressure measured by a humidity probe and P_s is the saturation water pressure. Relative pressures were varied from 0 to 1 in order to obtain the whole adsorption curve. Film pore volume was evaluated by adjusting the refractive index at $\lambda = 633$ nm with a two-medium Bruggeman effective medium approximation (BEMA), in $P = 0$ (dry nitrogen flux, air/silica) and $P = P_s$ (water saturated nitrogen flux, water/silica). Water uptake at intermediate pressures and pore size distributions were obtained by using WinElli 2 software (Sopra Inc.), which transforms the variation of n with P/P_s into filled pore volume by using a three-medium BEMA; pore size distributions are obtained according to a Kelvin model (13a).

Enzyme Immobilization. α-Amylase (from Bacillus Species) was purchased from Sigma-Aldrich and used as received. Its activity, as declared by the vendor, is 956 units (one unit is 1.0 mg of maltose produced from starch in 3 min at pH 6.9 at 20 °C per 1.0 mg of enzyme). Protein immobilization was achieved by immersing the so-prepared mesoporous films in a 0.1% enzyme aqueous solution for 60 min under agitation at room temperature. The films were then thoroughly rinsed with water and stored in a clean box at ambient conditions.

Evaluation of Enzyme Activity. The activities of the free enzyme and the biofunctionalized films were monitored by the well-known starch-iodine colorimetric method (14). Enzyme-containing samples or control experiments were incubated for 5 min in starch solutions (potato starch, from Fluka). The enzymatic reaction was quenched by addition of a stoichiometric (with respect to the initial starch concentration) amount of iodine (Aldrich). After 1/10 dilution in distilled water the absorbance at 620 nm was read in a Hewlett-Packard 8453 spectrophotometer. Control experiments, i.e., in the absence of the catalyst, were carried out as before. The percentage of degraded starch is given by: % SD $= (C - S)/C \times 100$, where C is the absorbance of the control and S is the absorbance of the sample.

All tests were carried out by immersing 1 cm^2 of biofunctionalized mesoporous silica films in 10 mL of starch solutions of different concentrations. The activity of the free enzyme was assessed by adding 1 mL of a 5 mg/L α-amylase solution to 9 mL 0.22% (mass percent) starch solution. Solution pH was fixed by small additions of HCl or NaOH.

Recycling test were also carried out as described. For this purpose, the functionalized mesoporous film stripes were removed from the reaction vessel, thoroughly washed with water, and reimmersed into fresh starch solutions.

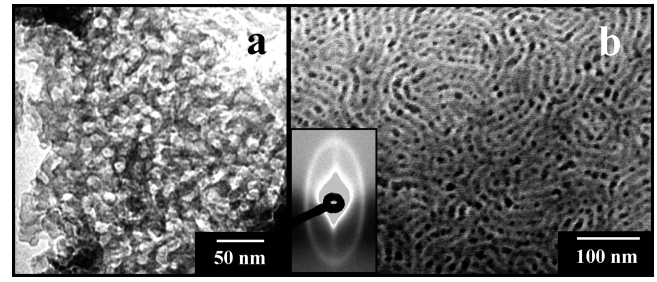

FIGURE 1. Top-view (a) TEM and (b) FE-SEM images of F127-templated mesoporous silica thin films. Inset: Representative 2D-SAXS pattern depicting the local order pore arrangement.

RESULTS AND DISCUSSION

Transparent, crack-free mesoporous thin films are obtained after the deposition−consolidation−calcination steps. Their thickness measured by XRR and ellipsometry are 85 and 135 nm for 1 and 2 mm s^{-1} withdrawal rates, respectively; both techniques yield the same result within the experimental uncertainty (<5%). Figure 1 shows FE-SEM and TEM micrographs of typical mesoporous silica thin films obtained under our synthesis conditions. They depict the homogeneous large-pore local order pore structure obtained using F127 as templating agent, as confirmed by SAXS information (see inset in Figure 1). The high surfactant/silica ratios used in this work−compared to [F127]/[Si] = 0.005 that leads to $Im\bar{3}m$ pore cubic symmetry (10) −ensure large pore size and good interconnectivity, in detriment of the local order of the pore system.

Figure 2 shows the H_2O-adsorption isotherm and pore size distribution of a representative mesoporous film measured by EEP, which exhibits a high pore volume; i.e., 48%. The shape of the pores of these mesoporous films resemble an array of ellipsoids interconnected by necks. Pore dimensions can be estimated from the adsorption branch of isotherms, according to ref 13a. A pore major diameter of 11 nm was derived, in good agreement with TEM pictures. For this type of interconnected mesopore systems, the desorption curve permits us to estimate the interpore neck diameter (15), which turned out to be 7 nm. The large size of the necks would allow for the incorporation of relatively

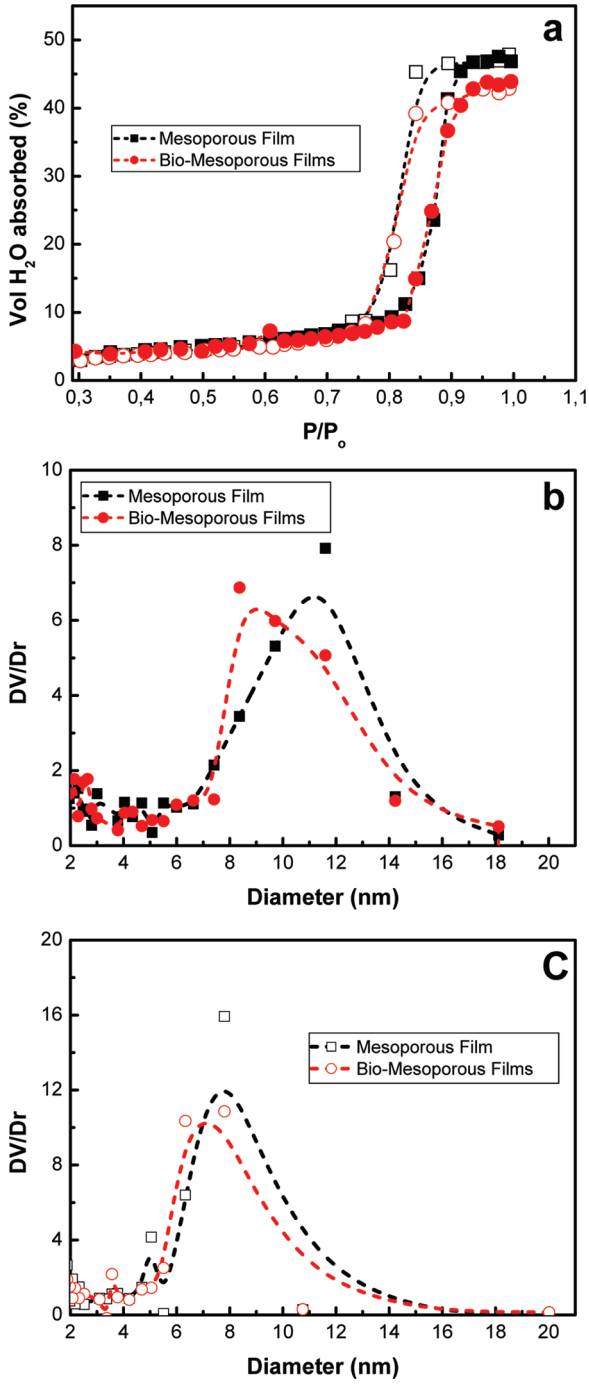

FIGURE 2. (a) Water adsorption−desorption isotherms obtained by EEP: (a) pore size distribution of mesoporous (black lines) and biofunctionalized (red lines) mesoporous thin films; (b) adsorption and (c) desorption isotherms. Dotted lines are guides to the eye.

large molecules, such as α-amylase, which can be geometrically described as an ellipsoid of dimensions 8.0 × 4.5 × 2.5 nm^3 (16). Mesoporous films exposed to α-amylase solutions and carefully washed present a marked increase of n_{700} at $P/P_s = 0$ with respect to the pristine mesoporous films ($\Delta n = 0.018$). This reflects a decrease in the pore volume, which must be ascribed to the incorporation of α-amylase within the mesopores. Considering that the volume fraction of the inorganic framework remains constant, and that the refractive index of α-amylase should be around 1.40, which is an average value used for most

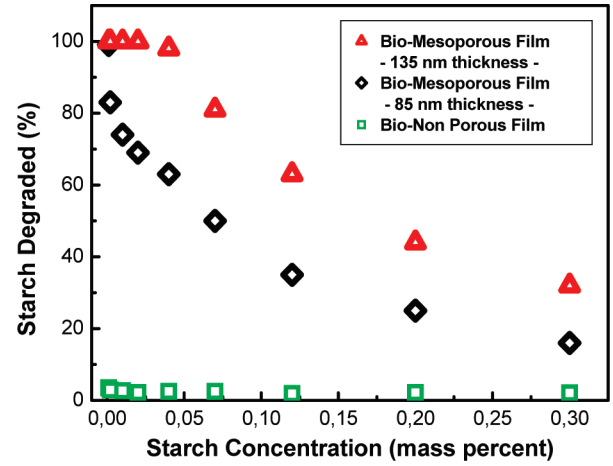

FIGURE 3. Effect of starch concentration on the percentage of starch degraded per 1 cm^2 of biofunctionalized films at 293 K and pH 6.

biomolecules and proteins (17), the volume fraction occupied by the enzyme can be estimated to be ∼ 4.3% on the basis of a three-component Bruggeman model. From Figure 2b, it is also apparent that the average diameters of pores and necks decrease after α-amylase immobilization. These facts suggest that there is a significant degree of pore occupancy by the enzymes; given that the volume of a α-amylase molecule is about one tenth of the volume of a pore, the observed reduction in porosity indicates that, on average, there would be one enzyme per pore. It is clear, however, that a substantial fraction of the pore volume remains accessible.

Direct determination of the amount of amylase incorporated within the films is indeed difficult. However, on the basis of the observed reduction of pore volume (4.3%), the molar volume of the enzyme (i.e., 47.1 nm^3 per molecule), and its molecular weight (ca. 51−54 kDa), the load of α-amylase in a 1 cm^2 area of a 135 nm thick film can be safely estimated to be about 1 μg.

The biofunctionalized mesoporous films, when immersed in starch solutions, show a significant capability to degrade starch (Figure 3). On the contrary, the activity of biofunctionalized non mesoporous silica films is negligible; mesoporous silica films alone (i.e., without enzymes) showed no catalytic activity. These results demonstrate that the combination of high surface area and accessible porosity of the mesoporous materials lead to an efficient entrapment of a large quantity of enzyme molecules that preserve their catalytic properties.

Figure 3 shows the percent of starch degraded after 5 min incubation at 20 °C for α-amylase-containing thin films put in contact with solutions containing different starch concentrations. Thicker films present substantially higher activity at every starch concentration. Importantly, the amount of degraded starch scales almost linearly with film thickness. This latter finding suggests that thicker films contain a larger quantity of enzyme that remain active irrespectively of the thickness. Clearly, α-amylase and the starch substrate are able to penetrate into the pore systems and to keep its activity while included within the pores; if the enzymes were located only at the film surfaces, the influence of film

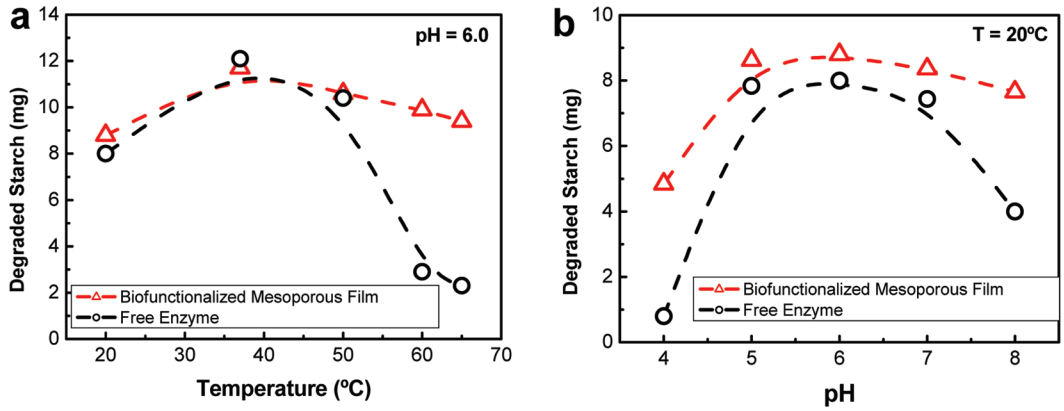

FIGURE 4. Influence of (a) temperature and (b) pH on the activity of 1 cm^2 of 135 nm thick biofunctionalized mesoporous thin films, and of 0.5 mg L^{-1} free amylase; starch concentration = 0.2%. Dotted lines are guides to the eye.

thickness would had been irrelevant. The large pore and neck sizes obtained under the present synthesis conditions grant the access of the rather large α-amylase molecules. It is interesting to observe that these open mesopore systems further allow processing a polymeric substrate, such as the carbohydrate chains of starch.

It is worth mentioning that enzyme uptake is a relatively fast process. Similar catalytic results were obtained after overnight immobilization of α-amylase. This reveals a rather rapid diffusion of the proteins within the mesoporous thin films, which again must be ascribed to the high accessibility and large pore size of the films. Obviously, they present more entrances to entrap large-size molecules than conventional mesoporous materials. It has been demonstrated that the morphology and pore system of mesoporous materials play an important role in their ability to immobilize enzymes (18).

To be able to integrate these biocatalytic films for advanced applications, it is desirable to generate enhanced resistance to extreme environmental conditions, such as pH and temperature. With the purpose of comparing the activities of the free and supported enzymes at different pH and temperature, the experimental conditions of the degradation tests were set in such a way that the resulting starch degradation at pH 6.0 and 20 °C were about 50%. This would offer a better appraisal of the catalytic performances of the enzyme and the functionalized film. Interestingly, at pH 6.0 and 20 °C, 1 cm^2 of a 135 nm thick biofunctionalized film degrades nearly the same amount of starch that 5 μg of free α-amylase does (Figure 4). Considering that the estimated amount of enzyme incorporated within the film mesopores is ca. 1 μg, this observation conveys the idea that the encapsulated enzymes bear an enhanced catalytic activity. If this estimation is correct, the specific activity of the functionalized film would be ca. 1,700 mg of degraded starch per mg amylase per minute, i.e., about 5 times larger than that of the free enzyme. Such an enhancement has already been reported for other confined enzymes (19). It seems likely that entrapment within the mesopores of the silica skeleton confers structural stability to α-amylase, thus preventing unfolding, hence ensuring the active site prone to react. At variance, however, it has been reported that immobilization of α-amylase into mesoporous silica particles renders a lesser enzymatic activity (20). It is possible, notwithstanding, that covalent anchoring of amylase would alter the structural conformation of the enzyme in a deleterious way (19d).

The overall kinetic mechanisms of enzymatic reactions taking place within mesoporous materials are by no means simple; all chemical, structural, and diffusional factors influence the measured overall rates. Diffusion of reactants/products through the intricate mesoporous network to/from the encaged enzymes is in itself a complex phenomenon that must not be overlooked. Unraveling the influence of each of the relevant kinetic factors, however, goes beyond the aim of the present work. Nonetheless, the observed enhanced enzymatic activity, and the noted proportional increase of degraded starch with film thickness, indicate that diffusion is not, in the present case, rate controlling. This conclusion further points out that appropriate tailoring of pore size, structure and interconnectivity of the mesoporous films is essential to overcome the obvious limitations posed by inner pore diffusion.

The activities of the free and immobilized enzyme at different temperatures and pH values are compared in Figure 4. In both cases, the maximum activity was achieved at ca. 37 °C (Figure 4a). Clearly, α-amylase immobilization buffers the effect of temperature, and the activity of the hybrid catalyst becomes significantly higher than that of the free enzyme as temperature increases. Likewise, enzyme immobilization renders higher activity at extreme pH values (Figure 4b). The observed trends further support the idea that α-amylase/pore inner surface interactions prevent enzyme unfolding. From the practical point of view, it is obvious that the use of the present biocatalytic films would relieve the rather stringent conditions that most processes based on free enzyme catalysis require.

Yet more importantly, the catalytic performance of these biofunctionalized mesoporous films does not deteriorate significantly on repeated use. Figure 5 shows that the catalyst remains fairly active up to 6 reaction cycles. The initial decrease in activity and the subsequent leveling off suggest that the slight lose in performance could be due to the detachment of a small fraction of α-amylase from the

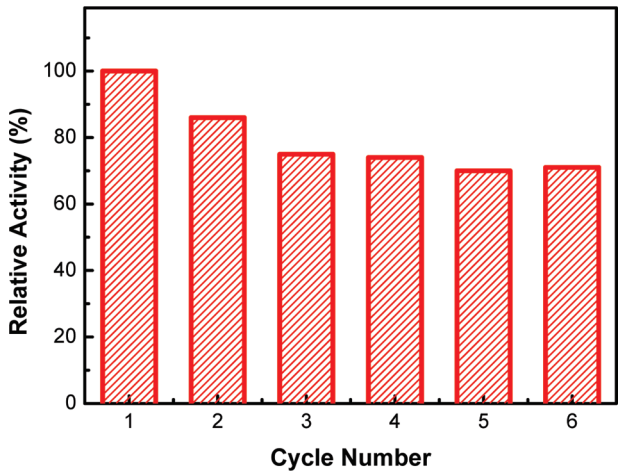

FIGURE 5. Activity of 1 cm^2 of a 135 nm thick biofunctionalized mesoporous thin film on repeated use; starch concentration = 0.2%; T = 293 K; pH 6.

outer film surface. Other effects, such as slow dissolution of the mesoporous silica support (21), may also be responsible for the observed trend. Despite the fact that enzyme functionalization may actually hinder dissolution of the inorganic matrix because protein adsorption should block active silanol sites, it can be argued that the instability of mesoporous silica thin films in aqueous media represents a liability of these biocatalysts for long-term applications. Nonetheless, our data clearly show that they are reusable, at least within a reasonable time frame, the simplest outcome being the substantial reduction of enzyme consumption.

In summary, we have reported the preparation of a robust biocatalyst that is active and stable, easy to handle, and simple to separate from the reaction medium. Furthermore, it can be used for several cycles. These biocatalytic strips showed excellent activity toward degradation of polymers, such as starch. From the technological point of view, they open a new gamut of applications, for enzymes are widely used in industry, as well as in biodiagnostics. Moreover, immobilization of enzymes in supported mesoporous thin films of appropriate pore architecture relieve the diffusional constraints usually faced by particulate biofunctionalized mesoporous materials. In addition, it renders catalyst recovery much easier.

It is worth remarking here the simplicity of the procedure used to prepare these biocatalyst stripes, especially when compared with one-pot enzyme functionalization sol−gel procedures (3), which require a very stringent control of the complex sol−gel chemistry that must be carefully adjusted to comply with the many kinetic factors that determine the activity of the entrapped enzymes. Our two-step approach decouples the engineering of the pore matrix (i.e., wall nature, pore size and symmetry, surface functions, etc.) from enzyme functionalization. In addition, the present applied methodology provides a platform to bioactive functionalization that is compatible with the techniques and substrates that are used in microelectronics. Indeed, mesoporous thin films can be easily patterned to gain lateral resolution, thus leading to biofunctionalized patterned mesoporous transparent films (22). Furthermore, their pore size distribution and connectivity can be tuned and tailored (23) to accommodate a whole variety of enzymes to meet specific applications. Finally, film-based enzyme supports are well-suited to a variety of industrial processes, comprising coatings, catalysts, optics, and sensors. An easy integration of these systems in food packaging, lab-on-chip, microfluidics, prosthetics, or bioMEMS can be anticipated.

Acknowledgment. Work funded by CONICET (PIP 5191) and ANPCyT (PICT 34518; PICT 00335; PAE 2004-22711, PAE 2006-37063-PME 00038). M.G.B. acknowledges a postdoctoral fellowship from CONICET. A.E.R. and G.J.A.A.S.-I. are staff members of CONICET and Gabbo's. The authors express their gratitude to Paula Angelomé and Cecilia Fuertes for their assistance in the characterization of the films. Thanks as well to Centro de Microscopías Avanzadas (FCEN-UBA) for the electron micrographs.

REFERENCES AND NOTES

(1) (a) Schoemaker, H. E.; Mink, D.; Wubbolts, M. G. *Science* **2003**, *299*, 1694. (b) Que, L.; Tolman, W. B. *Nature* **2008**, *455*, 333. (c) Woodley, J. M. *Trends Biotechnol.* **2008**, *26*, 321.

(2) (a) Cao, L. *Carrier-Bound Immobilized Enzymes: Principles, Application and Design*; Wiley-VCH: Weinheim, Germany, 2005. (b) BickerstaffG. F. *Immobilization of Enzymes and Cells*; Humana Press: Totowa, NJ, 1997. (c) Ma, J.; Zhang, L.; Liang, Z.; Zhang, W.; Zhang, Y. *J. Sep. Sci.* **2007**, *30*, 3050.

(3) (a) Johnson, P.; Whateley, T. L. *J. Colloid Interface Sci.* **1971**, *37*, 557. (b) Avnir, D.; Braun, S.; Lev, O.; Ottolenghi, M. *Chem. Mater.* **1994**, *6*, 1605. (c) Reetz, M. T.; Zonta, A.; Simpelkamp, J. *Angew. Chem., Int. Ed.* **1995**, *34*, 301. (d) Reetz, M. T. *Adv. Mater.* **1997**, *9*, 943. (e) Shtelzer, S.; Rappoport, S.; Avnir, D.; Ottolenghi, M.; Braun, S. *Biotechnol. Appl. Biochem.* **1992**, *15*, 227. (f) Livage, J.; Coradin, T.; Roux, C. *J. Phys.: Condens. Matter* **2001**, *13*, R673. (g) Avnir, D.; Coradin, T.; Lev, O.; Livage, J. *J. Mater. Chem.* **2005**, *16*, 1013. (h) Prouzet, E.; Ravaine, S.; Sanchez, C.; Backov, R. *New J. Chem.* **2008**, *32*, 1284. (i) Avnir, D.; Lev, O.; Livage, J. *J. Mater. Chem.* **2006**, *16*, 1013.

(4) (a) Mann, S.; Ozin, G. A. *Nature* **1996**, *382*, 313. (b) Soten, I.; Ozin, G. A. *Curr. Opin. Colloid Interface Sci.* **2000**, *5*, 325. (c) Ozin, G. A. *Chem. Commun.* **2000**, 419. (d) Sanchez, C.; Soler-Illia, G. J. A. A.; Ribot, F.; Lalot, T.; Mayer, C. R.; Cabuil, V. *Chem. Mater.* **2001**, *13*, 3061. (e) Soler-Illia, G. J. A. A.; Sanchez, C.; Lebeau, B.; Patarin, J. *Chem. Rev.* **2002**, *102*, 4093. (f) Soler-Illia, G. J. A. A.; Crepaldi, E. L.; Grosso, D.; Sanchez, C. *Curr. Opin. Colloid Interface Sci.* **2003**, *8*, 109.

(5) (a) Lee, C.-H.; Lin, T.-S.; Mou, C.-Y. *Nano Today* **2009**, *4*, 169. (b) Yiu, H. H. P.; Wright, P. A. *J. Mater. Chem.* **2005**, *15*, 3690. (c) Hartmann, M. *Chem. Mater.* **2005**, *17*, 4577.

(6) (a) Sanchez, C.; Boissière, C.; Grosso, D.; Laberty, C.; Nicole, L. *Chem. Mater.* **2008**, *20*, 682. (b) Soler-Illia, G. J. A. A.; Innocenzi, P. *Chem.—Eur. J.* **2006**, *12*, 4478. (c) Nicole, L.; Boissière, C.; Grosso, D.; Quach, A.; Sanchez, C. *J. Mater. Chem.* **2005**, *15*, 3598.

(7) (a) Xu, X.; Tian, B.; Kong, J.; Zhang, S.; Liu, B.; Zhao, D. *Adv. Mater.* **2003**, *12*, 1932. (b) Zang, X.; Wanga, J.; Wu, W.; Qiana, S.; Man, Y. *Electrochem. Commun.* **2007**, *9*, 2098.

(8) Kataoka, S.; Endo, A.; Oyama, M.; Ohmori, T. *Appl. Catal., A* **2009**, *359*, 108.

(9) (a) Uhlig, H.; Linsmaier-Bednar, E. M. *Industrial Enzymes and Their Applications*, John Wiley & Sons: New York, 1998. (b) Illanes, A. *Enzyme Biocatalysis: Principles and Applications*; Springer: Dordrecht, The Netherlands, 2008.

(10) (a) Angelomé, P. C.; Fuertes, M. C.; Soler-Illia, G. J. A. A. *Adv. Mater.* **2006**, *18*, 2397. (b) Cagnol, F.; Grosso, D.; Soler-Illia, G. J. A. A.; Crepaldi, E. L.; Babonneau, F.; Amenitsch, H.; Sanchez, C. *J. Mater. Chem.* **2003**, *13*, 61. (c) Fuertes, M. C.; López-Alcaraz, F. J.; Marchi, M. C.; Troiani, H. E.; Luca, V.; Míguez, H.; Soler-Illia, G. J. A. A. *Adv. Funct. Mater.* **2007**, *17*, 1247.

(11) Fuertes, M. C.; Marchena, M.; Marchi, M. C.; Wolosiuk, A.; Soler-Illia, G. J. A. A. *Small* **2009**, *5*, 272.

(12) Tompkins, H. G.; McGahan, W. A. *Spectroscopic Ellipsometry and Reflectometry: A User's Guide*; John Wiley & Sons: New York, 1999.

(13) (a) Boissière, C.; Grosso, D.; Lepoutre, S.; Nicole, L.; Brunet-Bruneau, A.; Sanchez, C. *Langmuir* **2005**, *21*, 12362. (b) Fuertes, M. C.; Colodrero, S.; Lozano, G.; Gonzalez-Elipe, A. R.; Grosso, D.; Boissière, C.; Sánchez, C.; Soler-Illia, G. J. A. A.; Míguez, H. *J. Phys. Chem. C* **2008**, *112*, 3157.
(14) (a) Smith, B. W.; Roe, J. H. *J. Biol. Chem.* **1949**, *179*, 53. (b) Smith, B. W.; Roe, J. H. *J. Biol. Chem.* **1957**, *227*, 357.
(15) Kim, T.-W.; Ryoo, R.; Kruk, M.; Gierszal, K. P.; Jaroniec, M.; Kamiya, S.; Terasaki, O. *J. Phys. Chem. B* **2004**, *108*, 11480.
(16) (a) Swift, H. J.; Brady, L.; Derewenda, Z. S.; Dodson, E.; Dodson, G. G.; Turkenburg, J. P.; Wilkinson, A. *Acta Crystallogr., Sect. B* **1991**, *47*, 535. (b) Bautista, L. F.; Martinez, M.; Aracil, J. *Ind. Eng. Chem. Res.* **2000**, *39*, 4320.
(17) Orosco, M. M.; Pacholski, C.; Sailor, M. J. *Nat. Nanotechnol.* **2009**, *4*, 255.
(18) (a) Fan, J.; Lei, J.; Wang, L.; Yu, C.; Tu, B.; Zhao, D. *Chem. Comm.* **2003**, 2140. (b) Sun, J.; Zhang, H.; Tian, R.; Ma, D.; Bao, X.; Su, D. S.; Zou, H. *Chem. Commun.* **2006**, 1322.
(19) (a) Fernandez-Lafuente, G.; Terreni, M.; Mateo, C.; Bastida, A.; Fernadez-Lafuente, R.; Dalmases, P.; Huguet, J.; Guisan, J. M. *Enzyme Microb. Technol.* **2001**, *28*, 389. (b) Lei, C.; Shin, Y.; Liu, J.; Ackerman, E. *J. Am. Chem. Soc.* **2002**, *124*, 11242. (c) Seelan, S.; Sinha, A. K.; Kato, K.; Yokogawa, Y. *Adv. Mater.* **2006**, *18*, 3001. (d) Zhang, Y.; Zhao, L.; Li, J.; Zhang, H.; Zheng, L.; Cao, S.; Li, C. *Biochem. Biophys. Res. Commun.* **2008**, *372*, 650.
(20) Pandya, H. P.; Jasra, R. V.; Newalkar, B. L.; Bhatt, P. N. *Microprous Mesoporous Mater.* **2005**, *77*, 67.
(21) Bass, J. D.; Grosso, D.; Boissiere, C.; Belamie, E.; Coradin, T.; Sanchez, C. *Chem. Mater.* **2007**, *19*, 4349.
(22) (a) Falcaro, P.; Costacurta, S.; Malfatti, L.; Takahashi, M.; Kidchob, T.; Casula, M. F.; Piccinini, M.; Marcelli, A.; Marmiroli, B.; Amenitsch, H.; Schiavuta, P.; Innocenzi, P. *Adv. Mater.* **2008**, *20*, 1864. (b) Innocenzi, P.; Kidchob, T.; Falcaro, P.; Takahashi, M. *Chem. Mater.* **2008**, *20*, 607.
(23) Malfatti, L.; Bellino, M. G.; Innocenzi, P.; Soler-Illia, G. J. A. A. *Chem. Mater.* **2009**, *21*, 2763.

AM900645B